Plastic burning particulate matter as a source of environmentally persistent free radicals and reactive oxygen and chlorine species

Check for updates

Rizana Salim[1,2,3], Sukriti Kapur[3], Meredith Schervish[3], Lena Gerritz[3], Kasey C. Edwards[3], Luis Ruis-Armenta[3], Emil Varghese[1,2], Raghunathan Ravikrishna[1,4], Sergey A. Nizkorodov[3], Sachin S. Gunthe[1,2] ✉ & Manabu Shiraiwa[3] ✉

Burning plastic waste releases massive amounts of atmospheric particulate matter (PM), but its chemical composition and health-related properties are largely unelucidated. Here we characterize chemical composition of PM generated from burning common types of plastics and quantify reactive oxygen/chlorine species and PM oxidative potential (OP). We find that plastic burning PM contains high levels of environmentally persistent free radicals (EPFRs), transition metals, and polycyclic aromatic hydrocarbons. In the aqueous phase, PM generates hydrogen peroxide, •OH radicals, and carbon-centered organic radicals, exhibiting high levels of OP as characterized by dithiothreitol (DTT) and OH assays. Remarkably, plastic burning PM is associated with high concentrations of hypochlorous acid. Kinetic model simulations demonstrate that the PM respiratory deposition leads to •OH formation via complex redox reactions among its constituents and antioxidants in lung lining fluid. Our study highlights significant atmospheric and health implications for unregulated plastic burning, particularly common in many areas of developing countries.

Plastics are ubiquitous polymeric materials that have become indispensable in daily life, with global plastic waste exceeding 52 million metric tonnes[1]. Plastic pollution is found globally and emissions of plastic are projected to increase in the future, emphasizing the need for collective global action[2]. Plastic wastes constitute nearly 12% of municipal solid waste and approximately 2 billion people discard them globally through process of open burning[3]. While incineration is a prevalent waste disposal method in urban areas and developed countries, practicing unregulated ways of disposal, mainly by burning, remains common in rural regions and developing countries[4]. India is the largest contributor to plastic waste, generating 9.3 million tons per year, surpassing China[1]. Nearly 66 to 93% of municipal solid waste, including plastic, is disposed into landfills in low- and medium-income countries[5] where intentional and unintentional fires are common in dump yards[6]. The combustion of plastics releases volatile organic compounds (VOCs) and particulate matter (PM) containing metals and polycyclic aromatic hydrocarbons (PAHs), which are known to be toxic to human health[7,8]. Plastic waste burning was reported to release approximately 0.92 ± 0.53 million tons of PM into the atmosphere globally in 2016[9] and this number may increase in future, if proper policies are not implemented for plastic waste management. Combustion processes mainly release fine PM[10], raising grave concerns for public health. It has been shown that plastic burning contributes significantly to fine PM, accounting for 13.4% of the total fine PM mass burden in New Delhi, India[11], 5–15% in Dhaka, Bangladesh[12], 6.8% in Nanjing, China[13], and 0.3–3% in Atlanta, USA[12]. Notably, plastic burning emissions characterized with high chloride contents have been identified as major cause of visibility reduction in Delhi[14]. A recent study highlighted the heightened toxicity of PM from commodity plastic burning compared to other waste types[9]. Open burning of plastics can also significantly contribute to the production of microplastics in the environment[15,16]. Despite awareness of the negative environmental and human health impacts of mismanagement of plastic waste, the chemical composition and health-related properties of plastic burning PM remain poorly understood.

[1]Centre for Atmospheric and Climate Sciences (CACS), Indian Institute of Technology Madras, Chennai, 600036, India. [2]Environmental Engineering division, Department of Civil Engineering, Indian Institute of Technology Madras, Chennai, 600036, India. [3]Department of Chemistry, University of California, Irvine, CA, 92697, USA. [4]Department of Chemical Engineering, Indian Institute of Technology Madras, Chennai, 600036, India. ✉e-mail: s.gunthe@iitm.ac.in; m.shiraiwa@uci.edu

Epidemiological studies have clearly linked the high concentrations of PM to adverse health impacts such as asthma, allergies, respiratory and cardiovascular diseases, and premature death[17]. Inhalation and respiratory deposition of PM can lead to the formation of reactive oxygen species (ROS) including hydroxyl radical ($\bullet$OH), superoxide radical ($\bullet O_2^-$), and hydrogen peroxide (H_2O_2) in the lung lining fluid[18]. Reactive chlorine species (RCS) including hypochlorous acid and hypochlorite anion ($HOCl/OCl^-$) have high oxidizing capability, acting as powerful microbicidal agents[19]. The excessive production of ROS and RCS can lead to adverse physiological effects by causing oxidative damage to biological molecules including lipids, proteins, and DNA to induce oxidative and chlorinative stress[20].

PM oxidative potential (OP) has received growing attention as an indicator of ROS generation and PM toxicity[21,22]. The dithiothreitol (DTT) assay is commonly used for probing redox-activity of PM and associated antioxidant depletion, which is sensitive to various compounds such as humic-like substances (HULIS), quinones, and transition metals[23]. High OP-DTT activity has been reported for ambient PM mainly affected by roadside trash burning in India[24]. The OP-OH assay measures the production rate of highly reactive $\bullet$OH in surrogate lung lining fluid containing major lung antioxidants[25]. Environmentally persistent free radicals (EPFRs) are long-lived radicals contained in PM, which are mainly emitted from incomplete combustion. EPFRs have extended lifetimes ranging from hours, days, and even to months, which facilitate their long-range transport and therefore increasing exposure risks[26,27]. EPFRs are shown to be redox-active to undergo redox cycling to generate ROS in the aqueous phase[28,29]. The presence of EPFRs has been observed in particulate soot and residue solid ash of burned polymeric material[30].
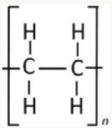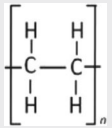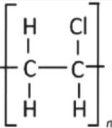
Little is known about the chemical composition, health-related properties, or toxicity of these emerging pollutants of plastic burning PM. In this study we generated PM by controlled combustion of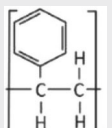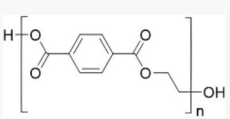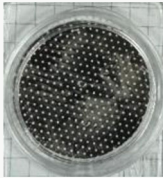 commonly used plastics and characterized their chemical composition including PAHs and transition metals. Further, we also quantified health-related properties including EPFRs, ROS, RCS, and OP. Our research aims to provide critical insights on induction of oxidative stress and aerosol health effects upon exposure and respiratory deposition of plastic burning PM, which will be crucial for implementing effective mitigation strategies, establishing air quality standards, and improving waste management practices.

Results
Chemical composition of plastic burning PM

We generated PM by controlled combustion of five types of plastics including low-density polyethylene (LDPE, often used for plastic bags), high-density polyethylene (HDPE, often used for plastic bottles and containers), polyvinylchloride (PVC, often used for pipes and cables), polystyrene (PS, often used for disposable cutlery and food packaging), and polyethylene terephthalate (PET, often used for containers of liquids and foods). Table 1 summarizes PM characteristics of each plastic type along with their chemical composition, structure and common uses. The

Table 1 | Characteristic properties of PM generated from plastic burning

Plastic	Chemical composition	Filter	Common uses	PM generated (g kg^{-1})
LDPE	$(C_2H_4)_n$		Plastic bags, containers, dispensing bottles, trays, general-purpose containers	3.6 ± 2.2
HDPE	$(C_2H_4)_n$		Milk jugs, detergent bottles, toys, shopping bags, juice and other liquid containers, caps and closures for bottles and jars	4.8 ± 0.7
PVC	$(CH_2-CH\text{-}Cl)_n$		Pipes, window frames, electrical cables, flooring, medical devices, automobile parts	17 ± 6
PS	$(CH_2-CH(C_6H_5))_n$		Disposable cutlery, food packaging, construction materials like insulation foams, toys, household appliances	22 ± 8
PET	$(C_{10}H_8O_4)_n$		Food packaging containers, packaging films, bottles for beverages, automobile and electronic parts	57 ± 14

Plastics with their commonly used names, chemical composition, the exemplary picture of filter used for collection of the PM for corresponding plastic, their common use, and PM emission factors.

combustion of different types of plastics was accompanied by flames and exhibited distinct characteristics in terms of colour and quantity of PM generated in the filters. Burning of PET produced thick black smoke and resulted in the filter used for sampling to be turning black, producing the highest amount of PM per mass of plastic burned with 57 ± 14 µg mg^{-1}. Filters from PVC burning appeared yellow to dark brown with a PM yield of 17 ± 6 µg mg^{-1}, while filters from PS burning appeared mostly black with a PM yield of 22 ± 8 µg mg^{-1}. Combustion of LDPE and HDPE results in a white residue and light-coloured filters, producing relatively low PM mass per mass of plastic burned with 4 ± 2 and 5 ± 1 µg mg^{-1}, respectively. Combustion of the other plastic has led to formation of black charred residue (Figure S1b).

Figure 1 shows the chemical composition including metals, PAHs and EPFRs for the PM from burning of five different plastics. Al was found to be the most abundant metal in LDPE and HDPE burning PM with concentration of ~4–7 µg mg^{-1}. PVC burning PM contains higher concentrations of Zn (9.4 µg mg^{-1}) and Cu (0.7 µg mg^{-1}), which is consistent with previous studies[30,31]. Zinc oxide is incorporated during the plastic manufacturing process as additives for thermal stabilisation and as colouring pigments[32]. Ni and Sb are found to be major components in PET and PS burning PM. The contribution of other minor metal components include Cr, Pb, and Cd, as also reported previously[33,34], whereas Fe was found to be below detection limit in any of our plastic burning PM.

PAHs are formed by incomplete combustion of organic materials, posing significant health risk as some of them are known to be carcinogens and mutagens. Total PAH concentration for different plastics are as follows: 61 ± 17 µg mg^{-1} for PS, 52 ± 1 µg mg^{-1} for PVC, 46 ± 16 µg mg^{-1} for HDPE, 39 ± 4 µg mg^{-1} for PET and 31 ± 7 µg mg^{-1} for LDPE. The identified PAHs mainly include naphthalene (NAP), fluorene (FLU), 9-fluorenone (9-FLU), phenanthrene (PHE), anthracene (ANTH), fluoranthene (FLT), benzanthracene (BaA), chrysene (CHR), benzo[b]fluoranthene (BbF), and benzo[a]pyrene (BaP), which aligns with findings from previous studies[30,35]. Figure S7 presents a stacked bar graph showing their concentrations and a pie chart illustrating their relative contributions to particulate matter from the combustion of individual plastic type. The concentration of individual PAHs identified in the PM is given in Table S1, along with the ratios of PAH isomers, which are often used for assessing source apportionment. The obtained ratios of ANTH/(ANTH + PHE)>0.1 and BaA/(BaA+CHR)>0.2 are consistent with the range of pyrolytic sources like biomass burning and other combustion sources, rather than petroleum sources[36,37]. Low molecular weight PAHs are typically produced during lower temperature processes like wood burning, while higher temperature processes, such as fuel combustion in engines, tend to emit higher molecular weight PAH compounds[36]. Further, to detect the functional groups in the PM, we derivatized the samples using N,O-Bis(trimethylsilyl)trifluoroacetamide (BSTFA). Terephthalic acid and hydroxybenzoic acid, which have been identified as two major plastic markers[35] are consistently detected in all our samples during analyses. In addition, we detected hydroquinones in PS burning PM and chlorophenols in PVC burning PM, including trichlorophenol, which is listed as a priority pollutant by the US Environmental Protection Agency (US EPA). Plastic burning PM may contain additional compounds that may be stemmed from additives such as plasticizers, colouring pigments, and UV/heat stabilizers; further studies are warranted to fully characterize highly complex chemical composition of plastic burning PM.

We found that all types of plastic burning PM contain significant amounts of EPFRs. The EPR spectra of all samples exhibited a single unstructured peak with g-values of ~2.0020 (Fig. S3), corresponding to carbon-centred organic radicals[26]. The concentrations of EPFRs are highest for PVC burning PM with 4.0 ± 1.3 pmol µg^{-1}, followed by PET with 1.9 ± 0.9 pmol µg^{-1}, LDPE with 1.8 ± 0.8 pmol µg^{-1}, PS with 0.70 ± 0.18 pmol µg^{-1}and HDPE with 0.15 ± 0.16 pmol µg^{-1}, respectively. For easier comparison, EPFR concentrations in Fig. 1a are presented in µg mg^{-1}, assuming a molecular weight of 200 g mol^{-1} for EPFRs[28]. These EPFR concentrations are comparable with previous measurements for wildfire

PM (~0.6 pmol µg^{-1})[38] and traffic PM (2.1–3.5 pmol µg^{-1})[39]. Elevated EPFR in PVC and PET burning PM may be due to the presence of functional groups including –Cl and –OH on aromatic rings, as these substituted phenolic compounds can form EPFRs by chemisorption on solid particles by dehydration or dehydrochlorination[40]. Most of the EPFRs that originate from combustion sources are phenoxy and semiquinone radicals which can be stabilized by transition metal oxides[10,41]. Cu(II)O, Ni(II)O, and Zn(II)O are known to produce and stabilize long-lived EPFRs[41,42]. While we did not find any correlation between Cu or Ni with EPFRs, we observed a strong positive correlation ($R^2 = 0.81$) between Zn and EPFRs (Fig. S4), suggesting that zinc oxides may contribute to the formation and stabilization of EPFRs in plastic burning PM.

Reactive oxygen and chlorine species

Figure 2a shows the representative EPR spectra of aqueous extracts of plastic burning PM. Each spectrum exhibits a combination of different radical species with the dashed vertical lines indicating the deconvoluted peaks for each type of BMPO radical adducts including •OH radicals (two conformers) and carbon-centred organic radicals. Figure 2b depicts relative contributions of each radical, showing that •OH is dominantly produced by LDPE and PET burning PM, whereas carbon-centred radicals are the major species for PS, PVC, and HDPE burning PM. Similar to these results, wildfire PM was reported to mainly generate •OH and carbon-centred radicals, but with a minor contribution from superoxide and oxygen-centred organic radicals[38].

Figure 2c shows the concentrations of ROS including total radicals and H_2O_2. We observe the highest yield of radicals for LDPE burning PM and the lowest yield by PVC burning PM. The observed total radical yields of ~0.01 – 0.2 pmol µg^{-1} are comparable to wildfire PM[38], which is much lower compared to radical yields by traffic PM[38,39]. Radical formation is a consequence of complex chemistry of chemical compounds which depends on burning materials and combustion conditions including temperature and availability of oxygen[38]. Figure 2c also shows the yields of H_2O_2 in the aqueous extract of the plastic burning PM. PVC burning PM yields the highest H_2O_2 (0.65 ± 0.43 pmol µg^{-1}), followed by PS burning PM (0.51 ± 0.38 pmol µg^{-1}). LDPE and HDPE burning PM yield 0.24 ± 0.10 and 0.29 ± 0.10 pmol µg^{-1} respectively, and PET burning PM exhibits the lowest yield with 0.07 ± 0.02 pmol µg^{-1}. The formation of H_2O_2 may be triggered by redox reactions of transition metals and quinones, alongside potentially other organic substances[43,44]. The yield of H_2O_2 is much higher than radicals, reflecting that H_2O_2 has longer lifetime as it is less reactive compared to radicals[45]. The differences in the type of ROS could be attributed to their distinct chemical composition and their different thermal decomposition products.

Figure 2c also shows HOCl yield in the aqueous extract of the plastic burning PM. The highest HOCl yield of 294 ± 13 pmol µg^{-1} was observed for PVC burning PM followed by PET burning PM with 112 ± 4 pmol µg^{-1}. Other three types of PM have relatively high HOCl yields of > 20 pmol µg^{-1}, which are a few orders of magnitude higher than H_2O_2 and radical yields. A previous study on composition of selected plastic packaging waste products reported presence of chlorine in their pyrolyzed samples of a variety of plastics including PE, PS and PET[46]. PVC is reported to have the highest chlorine content compared to other plastics[47], which is in line with highest HOCl yield by PVC burning PM. High HOCl yields imply that inhalation and respiratory deposition of plastic burning PM may cause chlorinative stress as HOCl is highly reactive to damage biological molecules including lipids, proteins, and nucleic acids[48]. Note that what we measured represent H_2O_2 and HOCl in aqueous extracts of PM and they should be regarded as lower limits of total yields as some of their fractions may have been volatilized during PM collection; the gas-phase measurements of HOCl and H_2O_2 are required for comprehensive quantification in future studies.

PM oxidative potential

Figure 3a shows oxidative potential of plastic burning PM as characterized by the decay of DTT (OP-DTT) and OH formation in surrogate lung fluid (OP-OH). These values are normalized with PM mass, representing an
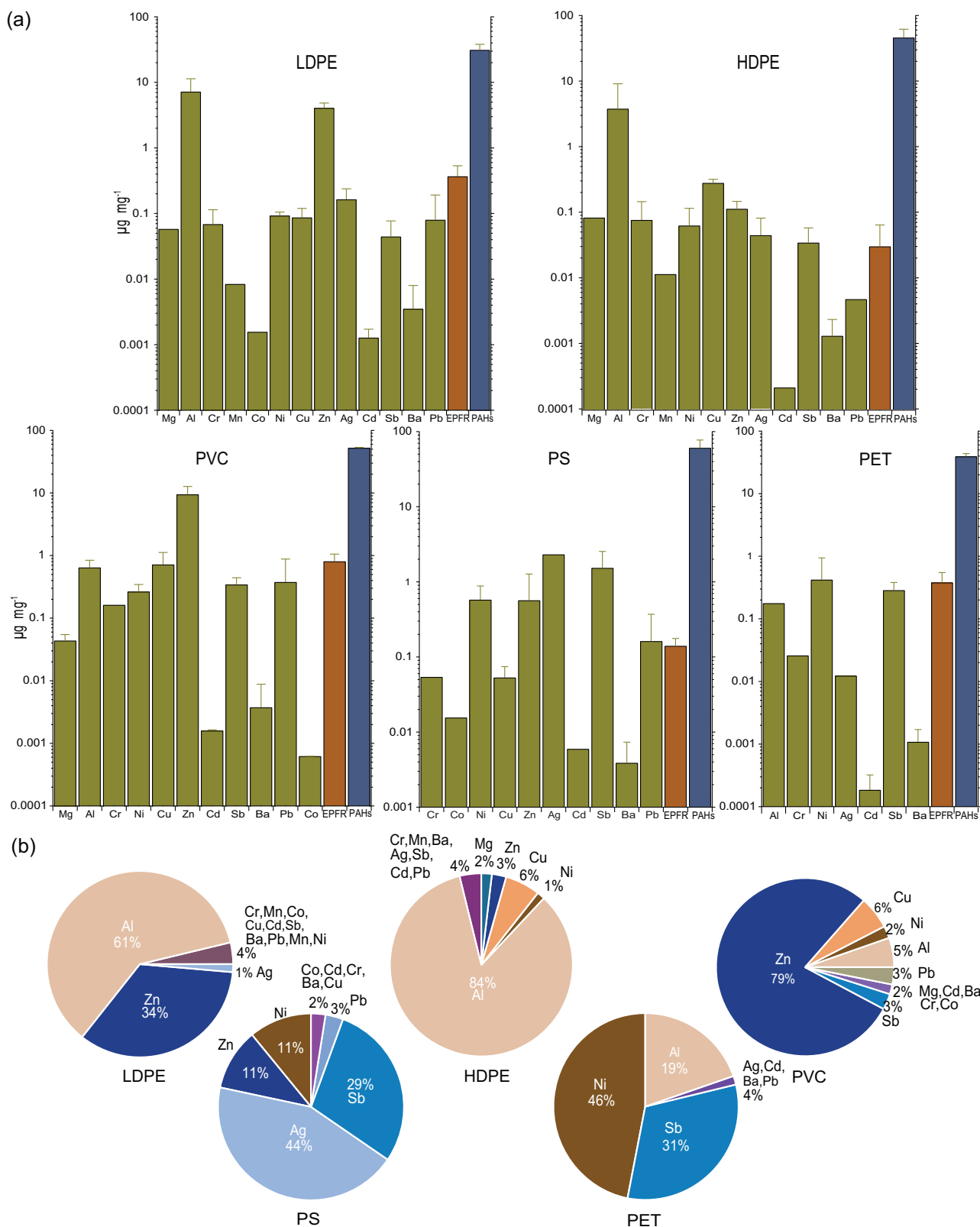
Fig. 1 | Characteristic properties of PM obtained from burning commonly used plastics. a The bar graph represents the concentrations of various metals, EPFRs and total PAHs in µg mg⁻¹ in PM as collected from the burning of LDPE, HDPE, PVC, PS and PET. Error bars represent the standard deviations (±1σ) representing the variations in the observed quantities of metals, EPFRs, and PAHs (N = 7 for EPFRs, N = 3 for metals and PAHs). The values without standard deviation are those where only one data point was considered as rest of the observations were below the detection limit. **b** Mass fraction of metals in different types of plastic burning PM.
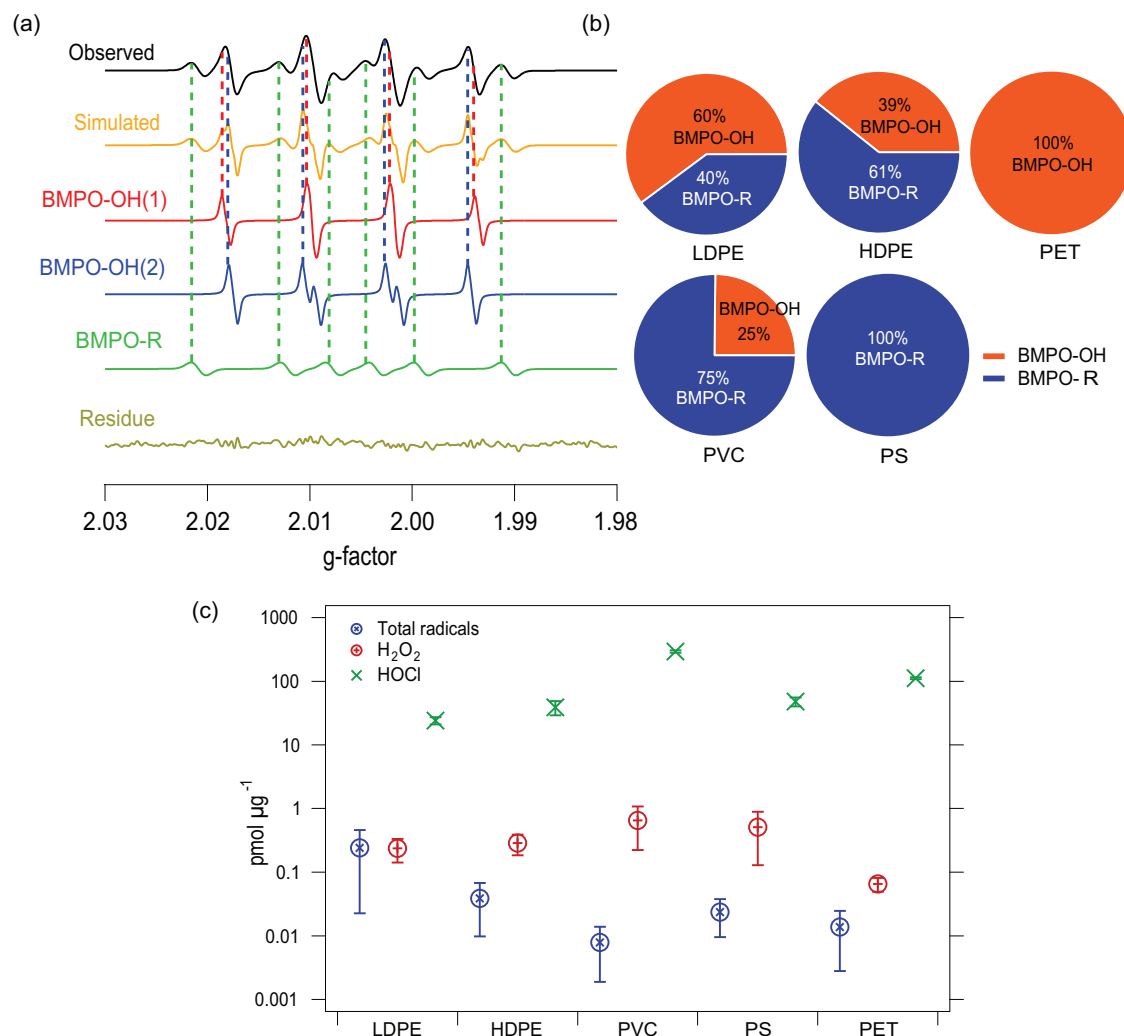
Fig. 2 | Quantification of reactive oxygen and chlorine species. a The observed and simulated EPR spectra of aqueous extracts of PVC burning PM deconvoluted to BMPO-OH (two conformers) and BMPO-R (carbon centred organic radicals) adducts. The dashed coloured-lines indicate peaks of BMPO- radical adducts. **b** Fractions of BMPO radical adducts (BMPO-OH and BMPO-R) in total radical formation in the aqueous extracts of different plastic burning PM represented in the form of pie-charts. **c** ROS comprising of total radicals (•OH and carbon-centred radicals), H_2O_2 and RCS (in the form of HOCl/OCl⁻) concentration in pmol μg⁻¹ in different plastic burning PM. All determinations are based on an average of at least three measurements samples with error bar showing one standard deviation.

intrinsic health-relevant property of PM. OP-DTT values are found to be high for PS and PVC burning PM with >110 pmol min⁻¹ μg⁻¹, followed by LDPE and PET burning PM, whereas HDPE burning PM exhibits low value of <10 pmol min⁻¹ μg⁻¹. These values are comparable with the average OP-DTT values of ambient PM in Delhi (~61 pmol min⁻¹ μg⁻¹)[49], Lahore (~19 pmol min⁻¹ μg⁻¹) and Peshawar (~28 pmol min⁻¹ μg⁻¹)[50], Los Angeles (~53 pmol min⁻¹ μg⁻¹)[25], Chicago (11–22 pmol min⁻¹ μg⁻¹)[51] and Atlanta (~24 pmol min⁻¹ μg⁻¹)[52]. OP-OH values exhibit similar trend with OP-DTT with PS and PVC burning PM showing higher OH generation with >1.3 pmol min⁻¹ μg⁻¹ [26], which are higher than ambient values in Los Angeles (0.48–0.63 pmol min⁻¹ μg⁻¹)[25] and sub-urban locations in China (0.2–1.2 pmol min⁻¹ μg⁻¹)[53].

Figure 3b shows that OP-DTT and OP-OH exhibit a strong correlation with $R^2 = 0.89$. This reflects that both assays are sensitive to similar but not exactly same compounds. In the inset is the scatter plot of average values of OP-DTT and OP-OH. The DTT assay is known to be sensitive to organic species such as redox-active quinones, HULIS and water-soluble metals including Cu but not with Fe, while the OP-OH assay is sensitive to Fe[23,25]. Both OP-DTT and OP-OH exhibit no significant correlations with PM mass (Fig. S9), confirming that PM oxidative potential is driven by chemical composition.

To further explore the relationship between OP and chemical composition, we performed a linear regression analysis between the OP and the observed concentrations of various metals, PAHs and EPFRs. Significant positive correlations are observed for total PAHs with OP-DTT and OP-OH (Fig. S10a). Despite PAHs not being redox-active themselves, their correlation with DTT loss could be attributed to close association of PAHs with redox-active quinones upon oxidation[54]. Among metals, antimony (Sb) and nickel (Ni) show significant positive correlations with OP-DTT and OP-OH (Fig. S10b, c). Ni is known to be redox active and sensitive to the DTT assay[55,56]. Sb is also redox active as has been recently shown that Sb can participate in redox reactions interacting with quinones[57]. We did not observe significant correlations with other redox-active metals including Zn and Cu (Fig. S10d, e). Furthermore, no significant correlation was found between OP and EPFR (Fig. S10f), suggesting EPFR is not a dominant factor for oxidative potential of plastic burning PM.

Kinetic modelling

Plastic burning PM is a complex mixture of a variety of organic compounds and transition metals. To understand the relationship between chemical composition of plastic burning PM with ROS formation and PM oxidative potential, we developed a kinetic box model to simulate •OH radical
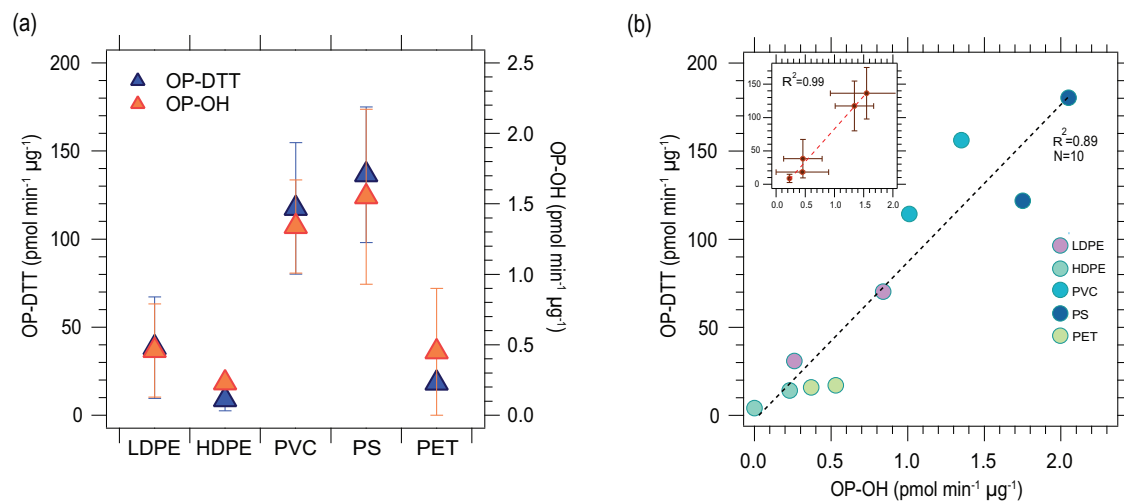
Fig. 3 | Oxidative potential of plastic burning PM. a Oxidative potential of the plastic burning PM assessed using the two acellular assays: OP-DTT and OP-OH. Results are reported in pmol min^{-1} µg^{-1}. Each measurement is conducted in triplicate, with error bars indicating one standard deviation. Out of the three measured samples for OP-OH, only one measurement was above background and hence not illustrated with error bars. **b** Scatter plot between OP-DTT and OP-OH is presented, with an inset showing the correlation of their average values with error bars extending to standard deviations (±1σ).
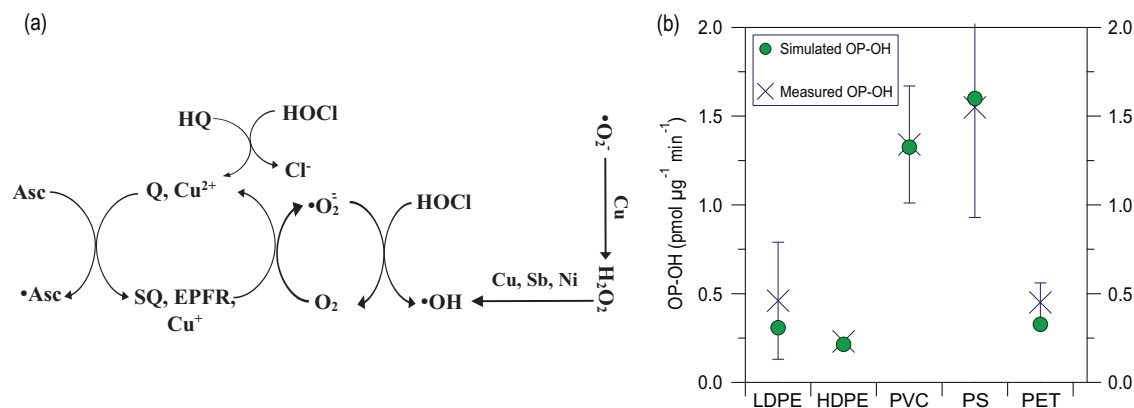

Fig. 4 | Reaction pathway in lung lining fluid for radical formation and oxidative potential of plastic burning PM. a The pathway involves redox cycling of EPFRs, quinones, metals such as Cu, Sb, Ni, reactive oxygen species such as •OH, •O$_2^-$, H$_2$O$_2$ and reactive chlorine species, HOCl. **b** Comparison of observed (dark blue markers) and modeled (green markers) production of •OH in lung lining fluid (OP-OH). Simulations are carried out with the reaction mechanism in Table S2. Error bars on each measurement represent one standard deviation. Out of the three measured samples for OP-OH, only one measurement was above background and hence not illustrated with error bars.

formation in surrogate lung fluid (OP-OH). The model treats redox cycling of redox-active components including quinones, EPFRs, and transition metal ions (Cu, Zn, Ni, Sb), ROS cycling, Fenton-like chemistry, and chlorine chemistry, building on previous studies[45,58], as shown in Fig. 4a. The mechanism involves several key processes contributing to ROS formation from plastic burning PM (see full mechanism in Table S2). Quinones and Cu(II) ion react with ascorbate to be reduced to semiquinones (SQ) and Cu(I) ion, which can react with dissolved O$_2$ to form superoxide (O$_2^-$)[45]. The chemical identity of EPFRs is considered to be semiquinone or phenoxy radicals, which are also redox-active to react with O$_2$ to form O$_2^-$. O$_2^-$ can be converted to H$_2$O$_2$ via ROS cycling reactions or reaction with Cu(I). Finally, •OH can be generated via Fenton-like reactions of transition metal ions with H$_2$O$_2$[45]. HOCl associated with PM can react with superoxide to form hydroxyl radicals[59], which is an additional pathway for the formation of •OH. The combined effects of the redox-active organic species, EPFRs, transition metals and chlorinated species lead to the release of a variety of highly reactive species with elevated OP-DTT and OP-OH values. In addition to ROS cycling and redox chemistry of metals and EPFRs, the model considers reactions of •OH with the organics known to be present in

plastics (see Fig. S11 for modelling results without this process). While the reactivity of •OH radical with organics depends on the structure and amount of specific organics present, we used a single rate coefficient for all the reactive organics to represent the average reactivity of •OH towards organics in plastic burning PM. We varied the amount of reactive organics in each type of plastic burning PM to achieve different reactivities of OH with the organics (see Fig. S11 for modelling results without this reaction).

Using this mechanism and constraints from the measurements, we are able to reproduce the OP-OH measurements within one standard deviation for the measured OP-OH for all types of PM (Fig. 4b). PVC burning PM has the highest concentrations of EPFRs, H$_2$O$_2$, HOCl, and Cu, all of which directly or indirectly lead to •OH formation. PS burning PM has a slightly higher OP-OH than PVC burning PM, as PS burning PM contains higher PAHs, which are used as a proxy for quinones, and thus can lead to more EPFR formation in the form of semiquinones. Additionally, PS burning PM has the highest total metal concentration (Cu, Ni, and Sb) leading to rapid Fenton-like chemistry to produce •OH from H$_2$O$_2$ even with the low concentration of Cu. Both total metals and PAHs show strong correlations with simulated OP-OH (Fig. S12). •OH formation is lower in PET burning

PM due to much lower Cu and H_2O_2. Moderate Sb, EPFR, and PAH concentrations in PET burning PM lead to moderate OP-OH activity. •OH formation in HDPE burning PM is limited by low EPFR concentrations and comparatively low total metals that participate in Fenton chemistry (Cu and Sb). LDPE has low total metals concentration (Cu, Sb and Ni), and PAHs with moderate EPFR and H_2O_2 concentrations, resulting in moderate OP-OH activity.

Overall, the •OH formation can be explained through complex chemistry involving redox cycling of redox-active components, ROS cycling, Fenton chemistry, and organic oxidation chemistry. The most critical parameters are the concentrations of redox-active metals that are able to participate in redox cycling and Fenton-like chemistry. These metals alone cannot explain the •OH formation. The H_2O_2 concentration or the ability to form H_2O_2 (via EPFR redox chemistry) is also critical leading to OP-OH not being dictated by or exhibiting a perfect linear relationship with any one given species.

Discussion

The ubiquity of plastics in everyday products has raised growing environmental concerns, particularly due to improper disposal methods such as open burning. India, the largest contributor to plastic waste emissions, faces significant challenges, with much of its waste being disposed of through uncontrolled burning, exacerbating the issue. Figure 5 depicts health and atmospheric implications of our findings of this study. Our results show that burning common plastics like PET, PVC, PS, LDPE, and HDPE releases PM containing harmful substances, including metals, PAHs, and EPFRs. Some of these components have the potential to induce ROS formation and hence, oxidative stress, a key mechanism in respiratory diseases, posing serious public health risks. PAHs are known to be toxic, and when they are aged in the atmosphere, they produce oxy- or nitro-PAHs, which are known mutagens and carcinogens[60], posing enhanced health risks. More studies are needed to understand toxicity and health effects of the plastic burning PM upon photochemical aging, as its oxidised products could have elevated toxicity. PS and PVC burning PM exhibit higher oxidative potential, as indicated by increased DTT and OH activity, both key indicators of PM toxicity. The presence of redox-active metals like Cu, Ni, and Sb may play a role in stabilizing EPFRs. EPFRs are redox-active and contribute to the generation of ROS in the aqueous phase. We observed a high production rate of •OH which can cause significant oxidative damage to biological molecules. It is remarkable to observe the formation of reactive chlorine species (RCS) in aqueous extracts of plastic burning PM. HOCl is a cytotoxic oxidant that can induce chlorinative stress that is linked to inflammation, disruption of antioxidant systems, tissue lesions, DNA damages, and apoptosis, which may lead to development of diseases like asthma, chronic obstructive pulmonary disease (COPD), and acute respiratory distress syndrome (ARDS)[61]. Our findings raise serious concerns about the short- and long-term health risks of acute and chronic exposure to emissions from plastic combustion, especially for vulnerable populations living near open burning sites. Further studies are warranted to evaluate toxicity and adverse health effects of plastic burning PM by cellular exposure and epidemiological studies.

In urban regions where unregulated plastic burning is prevalent such as in Delhi, the emissions from burning plastic contribute to the pollution of the environment. In addition to the release of toxic substances from plastic burning, these areas are also known to experience high emissions of nitrogen oxides (NOx) primarily from vehicular traffic. The combined effect of NOx emissions and the pollutants from plastic burning can have negative implications for local air quality and climate. For instance, high chloride emissions in Delhi, primarily from plastic burning, lead to the formation of ammonium chloride (NH_4Cl) particles in the presence of ammonia, which enhances aerosol water uptake to sustain particle growth, resulting in haze and reduced visibility[14]. High levels of HOCl associated with plastic burning PM found in this study implies that plastic burning can be an important source of HOCl in the troposphere, as HOCl can partition between the condensed and gaseous phase[62]. HOCl can react with nitrite ion (NO_2^-) in the condensed phase to form nitryl chloride ($ClNO_2$)[63]. The photolysis of $ClNO_2$ can lead to the formation of chlorine atom and NO_2, which can further photolyze to produce O_3[64]. High concentrations of $ClNO_2$, up to ~1 ppb, have been observed in polluted urban environments in China; chemical transport modelling has shown improved O_3 estimations when chlorine
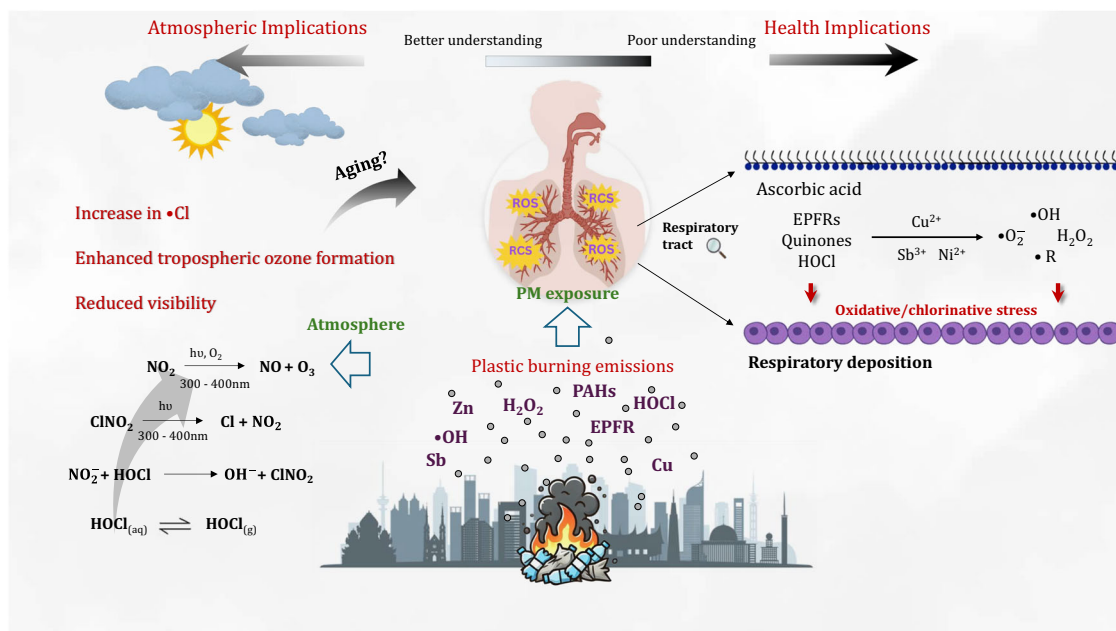

Fig. 5 | The impact of plastic burning emissions on local air quality and health. Schematic diagram showing the emissions of various pollutants from the plastic burning including PAHs, transition metals, and EPFRs. Respiratory deposition of PM can lead to the release of reactive oxygen species (ROS) and reactive chlorine species (RCS) in lung lining fluid to cause oxidative and chlorinative stress, possibly causing serious adverse health effects. Additionally, resulting environmental impacts due to chlorine emissions from plastic burning in the form of HOCl influencing the ozone chemistry. HOCl can significantly affect the visibility and air quality through chlorine and NO_X cycling.

chemistry is included[65]. Additionally, heterogeneous uptake of HOCl by organic aerosols, including biomass burning aerosols, can lead to the formation of organochlorides, which are generally toxic[66].

Our results suggests that plastic burning could be an important source for the reactive oxygen and chlorine species in the troposphere, which significantly affects the public health and regional air quality. Emissions of plastic burning PM can lead to an increase of the oxidizing capacity of the atmosphere by enhancing the formation of chlorine atoms and ozone. Accounting for local sources of chlorine emissions by plastic burning in air quality may result in improved estimation of ozone and other secondary pollutants, where observational data are in sparse. It is crucial to account for these emissions, especially in densely populated areas like Delhi, where unique meteorological and topographical factors, coupled with poor waste management practices, may exacerbate the issue. Additionally, the increasing frequency and intensity of wildfires in the wildland urban interface (WUI), such as the Marshall Fire in Colorado in 2021 and the Los Angeles wildfires in 2025, pose a growing concern. WUI fires lead to burning of vehicles and residential structures which contain substantial amounts of plastics[67]. Reducing the environmental and health risks of plastic burning requires strengthened waste management, stricter regulations, the adoption of sustainable alternatives, and updating the chemistry climate models with improved chemical mechanisms, in rapidly urbanising and densely populated regions.

Methods
PM generation
PM samples were generated by controlled combustion of commonly encountered plastics—low-density polyethylene (LDPE), high-density polyethylene (HDPE), polyvinylchloride (PVC), polystyrene (PS), and polyethylene terephthalate (PET) within a chamber equipped with a 2.5 cm diameter quartz tube and a Thermolyne 21135 tube furnace (Figure. S1a). The furnace was operated at 600 °C under a pressure of 750 Torr. The temperature of 600 °C falls within the typical range for polymer and plastic combustion and closely corresponds to commonly reported flame temperatures (600–750 °C)[30]. Each plastic type, approximately 200 mg, was placed in a ceramic crucible and positioned centrally within the quartz tube. Particle-free dry air was flushed through the tube at 1 L min^{-1} for 3–5 min, directing the combustion smoke through 47 mm filter holders where PM was collected on PTFE filters (Millipore, 0.2 μm pore size). Blank filters were collected prior to burning each plastic type, and thorough tube cleaning followed each experiment to remove any interferences between samples. Filters were weighed before and after PM collection using a microbalance. EPFR analysis was performed immediately after collection, and filters were subsequently stored at –20 °C for further analysis.

Radical measurements
A continuous wave electron paramagnetic resonance (CW-EPR) spectrometer (Bruker, Germany) was employed for identifying and quantifying the paramagnetic species in the plastic burning PM. The filters were folded and inserted into the quartz capillary of EPR (9.17 mm I.D., SP Wilmad- LabGlass) for the detection of EPFRs. The spectrometer was operated at a microwave frequency of 9.65 GHz; a microwave power of 36.18 mW (8 dB); a modulation frequency of 100 kHz; a modulation amplitude of 1.0 G; a receiver gain of 40 dB; a time constant of 10.24 ms; and a magnetic field scan of 1623.06 G. The concentration of EPFRs in the samples are reported in pmol μg^{-1}. EPFRs are quantified using the spin counting method embedded in Xenon software, and by comparing with the number of spins of standard, 4-hydroxy-2,2,6,6-tetramethylpiperidinyloxy (TEMPOL) (see calibration in Fig. S2).

EPR coupled with a spin-trapping technique is used for the detection and quantification of ROS. BMPO (5-tert-Butoxycarbonyl-5-methyl-1-pyrroline-N-oxide) (Enzo, ≥99%) is an efficient spin trap for OH, O$_2^-$ and organic radicals to form stable radical adducts. These radical adducts have long lifetime to be detected using EPR spectrometer. Depending on the mass collected on each filter, one-half or a quarter of a filter was used, where it was extracted into 10 mM BMPO in 200–300 μl Millipore water (>18 Ω cm^{-1})

and vortexed for 7 min using an analogue vortex mixer (VWR International LLC). The extracts were then concentrated to ~10 percent of volume by blowing under N$_2$ for 15-20 min and then loaded into a capillary tube for EPR measurements. EPR parameters used for ROS determination were same as EPFRs, except for the following: a microwave frequency of 9.86 GHz, a microwave power of 21.17 mW (10 dB); a time constant of 20.48 ms; a modulation amplitude of 1.0 G; and a magnetic field scan of 150.0 G. SpinFit and SpinCount modules with Xenon software were used to simulate and quantify the different BMPO radical adducts and deconvolute to their respective spectra. The ROS concentrations were normalized to the respective mass of PM and reported in pmol μg^{-1}.

Hydrogen peroxide fluorimetric assay
The quantification of H$_2$O$_2$ was done using the MAK 165 Fluorimetric Hydrogen Peroxide Assay Kit (Sigma-Aldrich), following the manufacturer's protocol as detailed in previous studies[68,69]. Briefly, a working solution was prepared with assay buffer, horseradish peroxidase, and red peroxidase. Samples were extracted in the assay buffer using an analogue vortex mixer (VWR International LLC) for 7 min. After extraction, samples were diluted with the working solution (0.06 ml), PBS (0.3 ml), and assay buffer to make the final volume of 3 ml. The addition of the working solution marked the beginning of the reaction, followed by an incubation period of 15 min at room temperature. Fluorescence measurements were conducted using a spectrofluorophotometer (RF-6000, Shimadzu) at excitation and emission wavelengths of 540 nm and 590 nm, respectively. Calibration was performed using H$_2$O$_2$ standards ranging from 1.5 to 0.05 μM, prepared by diluting with assay buffer as needed (see Figure. S5).

Hypochlorous acid fluorometric assay
Amplite® fluorimetric Hypochlorite (Hypochlorous Acid) assay kit from AAT bioquest was used for the quantification of hypochlorous acid. Briefly, filter samples were first extracted in the assay buffer for ~9 min. A calibration was performed using HOCl standard solutions, with concentrations from 0.001 to 100 mM by making the appropriate dilutions with the assay buffer (Fig. S6). A working solution of hypochlorite was prepared per the manufacturer's protocol. Along with the plastic samples, limonene SOA and 10 mM copper sulphate were also tested as negative controls. A volume of 50 μL of the working solution was added to hypochlorite standards or test samples (50 μL) to make the final volume 100 μL. Sample volumes of 100 μL were also tested without the addition of working solution to correct for background florescence. A volume of 50 μL of the working solution was added to hypochlorite standards or test samples (50 μL) to make the final volume 100 μL. The mixture was then incubated at room temperature for 10-30 min under dark condition. The addition of working solution was considered as the start of the reaction and the fluorescence was measured at emission and excitation wavelengths of 520 nm and 590 nm respectively using a microplate reader (Promega, GloMax). Values were corrected for background fluorescence, mass normalized and reported in pmol μg^{-1}. While this assay detects the total amount of HOCl and OCl$^-$, HOCl should be the dominant species, as pH of aqueous extracts of plastic burning PM was in the range of ~6–7 and the pK$_a$ value of HOCl is 7.5.

Metals - ICP-MS
Metals in the sample were determined by inductively coupled plasma mass spectrometry (ICP-MS) (Thermo Scientific™ iCAP™ RQ single quadrupole (SQ) ICP-MS). Calibration standards CMS-4 and CMS-5 (inorganic ventures) were used for the selected metals-As, B, Ba, Cd, Sb, Se, Ag, Al, Ca, Co, Cr, Cu, Fe, Mg, Mn, Na, Ni, Zn. The filters were extracted using a vortex shaker for 10 min into 2 ml HNO$_3$ (69%) and sonicated for 1 h. The solution was diluted with DI water to make a final concentration of ~1%. Measurements were carried out in triplicate and results reported in μg mg^{-1}.

Polycyclic aromatic hydrocarbons—GC-MS
The PAHs in the samples were detected using gas-chromatography mass-spectrometry (Thermo Triplus Ultra GC-MS). The focus was given to the

PAHs that are designated as priority pollutant PAHs by US EPA and the following PAHs were found in the plastic burning PM: naphthalene, fluorene, 9-fluorenone, phenanthrene, anthracene, fluoranthene, benzanthracene, chrysene, benzo[b]fluoranthene, and benzo[a]Pyrene. Briefly, the filters were extracted into 1 ml DCM using vortex shaker (vortex genie) followed by centrifugation to remove the non-soluble fraction. Samples were injected (10 μL injection volume, PTV-splitless) at 80 °C and separated on a 30 m DB-5MS column (Agilent) with a constant gradient of $20\,°C\,min^{-1}$ from 40 to 310 °C with a 5 min hold at 310 °C. Species were detected via electron impact ionization at 250 °C on a single quadrupole mass spectrometer (ISQ, Thermo Scientific) from m/z 30–650. The data was acquired and processed using the Chromeleon 7 software and individual PAHs were identified by comparison with the NIST MS search 2.3 library. The identity of select PAHs was confirmed and quantified using authentic standards. The calibration curves given in Fig. S7a were further used for the quantification of the selected PAHs (Fig. S7 b). Triplicate measurements were conducted to report results in $μg\,mg^{-1}$.

PM oxidative potential

We measured total DTT activity of plastic burning PM. To measure the total DTT, the filters were extracted into 1.4 ml of Milli Q water using a vortex shaker. The extracts with the filters were used in the subsequent steps for measuring the total DTT activity including both soluble and insoluble components. In the incubation vials, 0.7 mL samples or blank and 0.2 mL of 0.5 M Chelex-treated potassium phosphate buffer (to maintain pH at 7.4) were incubated at 37 °C. Addition of 100 μL of 1 mM DTT to the incubation vials was considered as the start of the reaction. At designated time points, a 50 μL aliquot was removed and added to a centrifuge tube preloaded with 0.5 mL 1% trichloroacetic acid (TCA) to quench the DTT consumption. Then, 1 mL Tris buffer, 0.25 mL of 0.2 mM 5,5′-dithiobis(2-nitrobenzoic acid (DNTB) and 10 mL deionozed water were added and absorbance was measured at 412 nm. Absorbance was also measured at 600 nm for background correction.

In OP-OH assay, •OH formation was measured in surrogate lung fluid (SLF). The SLF was composed of 2.5 mM ascorbic acid, 1.25 mM reduced glutathione and 1.25 mM uric acid in 50 ml of phosphate-buffered saline. The filters were vortexed in SLF with disodium terephthalate (TPT) for 7 min with a vortex shaker. TPT reacts with OH radicals to form 2-hydroxy terephthalic acid (2-OHTA), which is highly fluorescent. The extracts were incubated for 30, 60, 90 and 120 min and 2-OHTA was quantified at 320/420 nm using a fluorescence spectrometer (Shimadzu). Calibration is performed using 2-OHTA standards at concentrations in the range of 100 nM–8 μm (Fig. S8).

Kinetic modelling

The concentration of the fluorescent molecule (2-OHTA) in the OP-OH assay is simulated using a kinetic model. This model includes redox chemistry of antioxidants in surrogate lung fluid, EPFRs, HOCl, and metals as well as ROS cycling and Fenton-like chemistry. A schematic of this chemistry is shown in Fig. 4 and the full list of reactions simulated and their rate coefficients are given in the Table S2. Where available, rate coefficients are taken from literature. Fenton chemistry involving nickel is assumed to proceed with the same rate coefficient as copper as the rate coefficient is not available in literature. Concentrations of EPFR, HOCl, PAH, Cu, Ni, Sb, and H_2O_2 were used as model inputs. The total PAH concentration is used as the initial value for quinones. While the PAH concentration is not equivalent to the quinone concentration as the yield of quinones from varies with different PAHs, this provides a rough estimate for a highly uncertain value[70]. All species were treated as soluble and homogeneously mixed in aqueous PM extracts. Such an assumption may not be appropriate for metals, which can be present as insoluble oxides, but was made to reduce complexity and minimize tunable parameters, as only total metal measurements were available and water solubility of metals is highly uncertain. A series of odes based on the reactions given in the SI are automatically generated and solved using MATLAB's built-in ode solvers. The reaction of OH with TPT to form

2-OHTA is simulated and divided by the total simulation time to achieve a formation rate in order to compare to measured OP-OH values.

Data availability
Data can be obtained from the corresponding author upon reasonable request.

Code availability
The model code is available from the corresponding author upon reasonable request.

References

1. Cottom, J. W., Cook, E. & Velis, C. A. A local-to-global emissions inventory of macroplastic pollution. *Nature* **633**, 101–108 (2024).
2. MacLeod, M., Arp, H. P. H., Tekman, M. B. & Jahnke, A. The global threat from plastic pollution. *Science* **373**, 61–65 (2021).
3. Velis, C. A. & Cook, E. Mismanagement of plastic waste through open burning with emphasis on the Global South: A systematic review of risks to occupational and public health. *Environ. Sci. Technol.* **55**, 7186–7207 (2021).
4. Ferronato, N. & Torretta, V. Waste mismanagement in developing countries: A review of global issues. *Int. J. Environ. Res. Public. Health* **16**, 1060 (2019).
5. Sharma, K. D. & Jain, S. Municipal solid waste generation, composition, and management: the global scenario. *Soc. Responsib. J.* **16**, 917–948 (2020).
6. Pathak, G., et al. Plastic pollution and the open burning of plastic wastes. *Glob. Environ. Change* **80**, 102648 (2023).
7. Lemieux, P. M., Lutes, C. C. & Santoianni, D. A. Emissions of organic air toxics from open burning: a comprehensive review. *Prog. Energy Combust. Sci.* **30**, 1–32 (2004).
8. Wiedinmyer, C., Yokelson, R. J. & Gullett, B. K. Global emissions of trace gases, particulate matter, and hazardous air pollutants from open burning of domestic waste. *Environ. Sci. Technol.* **48**, 9523–9530 (2014).
9. Wu, D. et al. Commodity plastic burning as a source of inhaled toxic aerosols. *J. Hazard. Mater.* **416**, 125820 (2021).
10. Cormier, S. A., Lomnicki, S., Backes, W. & Dellinger, B. Origin and health impacts of emissions of toxic by-products and fine particles from combustion and thermal treatment of hazardous wastes and materials. *Environ. Health Perspect.* **114**, 810–817 (2006).
11. Gadi, R., Shivani, Sharma, S. K. & Mandal, T. K. Source apportionment and health risk assessment of organic constituents in fine ambient aerosols (PM2.5): A complete year study over National Capital Region of India. *Chemosphere* **221**, 583–596 (2019).
12. Islam, Md.R., Welker, J., Salam, A. & Stone, E. A. Plastic burning impacts on atmospheric fine particulate matter at urban and Rural Sites in the USA and Bangladesh. *ACS Environ. Au* **2**, 409–417 (2022).
13. Haque, M.Md. et al. Characterization of organic aerosols from a Chinese megacity during winter: predominance of fossil fuel combustion. *Atmos. Chem. Phys.* **19**, 5147–5164 (2019).
14. Gunthe, S. S. et al. Enhanced aerosol particle growth sustained by high continental chlorine emission in India. *Nat. Geosci.* **14**, 77–84 (2021).
15. Hess, K. Z. et al. Emerging investigator series: Open dumping and burning: an overlooked source of terrestrial microplastics in underserved communities. *Environ. Sci. Process. Impacts* **27**, 52–62 (2025).
16. Luo, Y. et al. Fire releases micro- and nanoplastics: Raman imaging on burned disposable gloves. *Environ. Pollut.* **312**, 120073 (2022).
17. Cohen, A. J. et al. Estimates and 25-year trends of the global burden of disease attributable to ambient air pollution: an analysis of data from

the Global Burden of Diseases Study 2015. *Lancet* **389**, 1907–1918 (2017).

18. Shiraiwa, M. et al. Aerosol health effects from molecular to global scales. *Environ. Sci. Technol.* **51**, 13545–13567 (2017).

19. Gray, M., Wholey, W.-Y. & Jakob, U. Bacterial responses to reactive chlorine species. *Annu. Rev. Microbiol.* **67**, 141–160 (2013).

20. Winterbourn, C. C. Reconciling the chemistry and biology of reactive oxygen species. *Nat. Chem. Biol.* **4**, 278–286 (2008).

21. Bates, J. T. et al. Review of acellular assays of ambient particulate matter oxidative potential: Methods and relationships with composition, sources, and health effects. *Environ. Sci. Technol.* **53**, 4003–4019 (2019).

22. Daellenbach, K. R. et al. Sources of particulate-matter air pollution and its oxidative potential in Europe. *Nature* **587**, 414–419 (2020).

23. Gao, D., Ripley, S., Weichenthal, S. & Godri Pollitt, K. J. Ambient particulate matter oxidative potential: Chemical determinants, associated health effects, and strategies for risk management. *Air Pollut. Conséq. Cell. Redox Signal. Antioxid. Def. Dis.* **151**, 7–25 (2020).

24. Vreeland, H. et al. Chemical characterization and toxicity of particulate matter emissions from roadside trash combustion in urban India. *Atmos. Environ.* **147**, 22 (2016).

25. Shen, J. et al. Aerosol oxidative potential in the Greater Los Angeles Area: Source apportionment and associations with socioeconomic position. *Environ. Sci. Technol.* **56**, 17795–17804 (2022).

26. Dellinger, B. et al. Formation and stabilization of persistent free radicals. *Proc. Combust. Inst.* **31**, 521–528 (2007).

27. Gehling, W. & Dellinger, B. Environmentally persistent free radicals and their lifetimes in $PM_{2.5}$. *Environ. Sci. Technol.* **47**, 8172–8178 (2013).

28. Edwards, K. C. et al. Residential wood burning and vehicle emissions as major sources of environmentally persistent free radicals in Fairbanks, Alaska. *Environ. Sci. Technol.* **58**, 14293–14305 (2024).

29. Khachatryan, L., Vejerano, E., Lomnicki, S. & Dellinger, B. Environmentally persistent free radicals (EPFRs). 1. Generation of reactive oxygen species in aqueous solutions. *Environ. Sci. Technol.* **45**, 8559–8566 (2011).

30. Valavanidis, A., Iliopoulos, N., Gotsis, G. & Fiotakis, K. Persistent free radicals, heavy metals and PAHs generated in particulate soot emissions and residue ash from controlled combustion of common types of plastic. *J. Hazard. Mater.* **156**, 277–284 (2008).

31. Hubai, K. et al. Phytotoxicity of particulate matter from controlled burning of different plastic waste types. *Bull. Environ. Contam. Toxicol.* **109**, 852–858 (2022).

32. Turner, A. & Filella, M. Hazardous metal additives in plastics and their environmental impacts. *Environ. Int.* **156**, 106622 (2021).

33. Kováts, N. et al. Ecotoxic emissions generated by illegal burning of household waste. *Chemosphere* **298**, 134263 (2022).

34. Park, Y. K., Kim, W. & Jo, Y. M. Release of Harmful Air Pollutants from Open Burning of Domestic Municipal Solid Wastes in a Metropolitan Area of Korea. *Aerosol Air Qual. Res.* **13**, 1365–1372 (2013).

35. Simoneit, B. R. T., Medeiros, P. M. & Didyk, B. M. Combustion Products of Plastics as Indicators for Refuse Burning in the Atmosphere. *Environ. Sci. Technol.* **39**, 6961–6970 (2005).

36. Tobiszewski, M. & Namieśnik, J. PAH diagnostic ratios for the identification of pollution emission sources. *Environ. Pollut.* **162**, 110–119 (2012).

37. Yunker, M. B. et al. PAHs in the Fraser River basin: a critical appraisal of PAH ratios as indicators of PAH source and composition. *Org. Geochem.* **33**, 489–515 (2002).

38. Fang, T. et al. Wildfire particulate matter as a source of environmentally persistent free radicals and reactive oxygen species. *Environ. Sci. Atmos.* **3**, 581–594 (2023).

39. Hwang, B. et al. Environmentally persistent free radicals, reactive oxygen species generation, and oxidative potential of highway $PM_{2.5}$. *ACS Earth Space Chem.* **5**, 1865–1875 (2021).

40. Pan, B., Li, H., Lang, D. & Xing, B. Environmentally persistent free radicals: Occurrence, formation mechanisms and implications. *Environ. Pollut.* **248**, 320–331 (2019).

41. Vejerano, E. P., Rao, G., Khachatryan, L., Cormier, S. A. & Lomnicki, S. Environmentally Persistent Free Radicals: Insights on a New Class of Pollutants. *Environ. Sci. Technol.* **52**, 2468–2481 (2018).

42. Patterson, M. C. et al. Formation of environmentally persistent free radicals (EPFRs) on ZnO at room temperature: Implications for the fundamental model of EPFR generation. *Chem. Phys. Lett.* **670**, 5–10 (2017).

43. Shen, H., Barakat, A. I. & Anastasio, C. Generation of hydrogen peroxide from San Joaquin Valley particles in a cell-free solution. *Atmos. Chem. Phys.* **11**, 753–765 (2011).

44. Tong, H. et al. Aqueous-phase reactive species formed by fine particulate matter from remote forests and polluted urban air. *Atmos. Chem. Phys.* **21**, 10439–10455 (2021).

45. Lakey, P. S. J. et al. Chemical exposure-response relationship between air pollutants and reactive oxygen species in the human respiratory tract. *Sci. Rep.* **6**, 32916 (2016).

46. Roosen, M. et al. Detailed Analysis of the Composition of Selected Plastic Packaging Waste Products and Its Implications for Mechanical and Thermochemical Recycling. *Environ. Sci. Technol.* **54**, 13282–13293 (2020).

47. López, A., de Marco, I., Caballero, B. M., Laresgoiti, M. F. & Adrados, A. Dechlorination of fuels in pyrolysis of PVC containing plastic wastes. *III Int. Congr. Energ. Eng. Environ.* **92**, 253–260 (2011).

48. Yap, Y. W., Whiteman, M. & Cheung, N. S. Chlorinative stress: An under appreciated mediator of neurodegeneration?. *Cell. Signal.* **19**, 219–228 (2007).

49. Verma, P. K. et al. Summertime oxidative potential of atmospheric PM2.5 over New Delhi: Effect of aerosol ageing. *Sci. Total Environ.* **920**, 170984 (2024).

50. Ahmad, M. et al. Chemical characteristics, oxidative potential, and sources of PM2.5 in wintertime in Lahore and Peshawar, Pakistan. *J. Environ. Sci.* **102**, 148–158 (2021).

51. Yu, H., Puthussery, J. V. & Verma, V. A semi-automated multi-endpoint reactive oxygen species activity analyzer (SAMERA) for measuring the oxidative potential of ambient $PM_{2.5}$ aqueous extracts. *Aerosol Sci. Technol.* **54**, 304–320 (2020).

52. Gao, D., Mulholland, J. A., Russell, A. G. & Weber, R. J. Characterization of water-insoluble oxidative potential of PM2.5 using the dithiothreitol assay. *Atmos. Environ.* **224**, 117327 (2020).

53. Li, X. et al. Oxidative Potential by $PM_{2.5}$ in the North China Plain: Generation of Hydroxyl Radical. *Environ. Sci. Technol.* **53**, 512–520 (2019).

54. Cho, A. K. et al. Redox activity of airborne particulate matter at different sites in the Los Angeles Basin. *Environ. Res.* **99**, 40–47 (2005).

55. Charrier, J. G. & Anastasio, C. On dithiothreitol (DTT) as a measure of oxidative potential for ambient particles: evidence for the importance of soluble transition metals. *Atmos. Chem. Phys.* **12**, 9321–9333 (2012).

56. Geller, M. D. et al. Physicochemical and redox characteristics of particulate matter (PM) emitted from gasoline and diesel passenger cars. *Atmos. Env.* **40**, 6988 (2006).

57. Rong, Q., Zhang, C., Ling, C., Lu, D. & Jiang, L. Mechanism of extracellular electron transport and reactive oxygen mediated Sb(III) oxidation by Klebsiella aerogenes HC10. *J. Environ. Sci.* **147**, 11–21 (2025).

58. Rodríguez, E. M. & von Gunten, U. Generation of hydroxyl radical during chlorination of hydroxyphenols and natural organic matter extracts. *Water Res.* **177**, 115691 (2020).

59. Liou, S.-Y. & Dodd, M. C. Evaluation of hydroxyl radical and reactive chlorine species generation from the superoxide/hypochlorous acid reaction as the basis for a novel advanced oxidation process. *Water Res.* **200**, 117142 (2021).

60. Clergé, A., Le Goff, J., Lopez, C., Ledauphin, J. & Delépée, R. Oxy-PAHs: occurrence in the environment and potential genotoxic/mutagenic risk assessment for human health. *Crit. Rev. Toxicol.* **49**, 302–328 (2019).

61. Casciaro, M. et al. Chlorinative stress in age-related diseases: a literature review. *Immun. Ageing* **14**, 21 (2017).

62. Lawler, M. J., et al. HOCl and Cl$_2$observations in marine air. *Atmos. Chem. Phys.* **11**, 7617–7628 (2011).

63. Dalton, E. Z. et al. Daytime Atmospheric Halogen Cycling through Aqueous-Phase Oxygen Atom Chemistry. *J. Am. Chem. Soc.* **145**, 15652–15657 (2023).

64. Thornton, J. A. et al. A large atomic chlorine source inferred from mid-continental reactive nitrogen chemistry. *Nature* **464**, 271–274 (2010).

65. Hong, Y. et al. The role of anthropogenic chlorine emission in surface ozone formation during different seasons over eastern China. *Sci. Total Environ.* **723**, 137697 (2020).

66. Jorga, S. D. et al. Kinetics of hypochlorous acid reactions with organic and chloride-containing tropospheric aerosol. *Environ. Sci. Process. Impacts* **25**, 1645–1656 (2023).

67. Holder, A. L., Ahmed, A., Vukovich, J. M. & Rao, V. Hazardous air pollutant emissions estimates from wildfires in the wildland urban interface. *PNAS Nexus* **2**, pgad186 (2023).

68. Wei, J. et al. Superoxide formation from aqueous reactions of biogenic secondary organic aerosols. *Environ. Sci. Technol.* **55**, 260–270 (2021).

69. Tong, H. et al. Reactive oxygen species formed by secondary organic aerosols in water and surrogate lung fluid. *Environ. Sci. Technol*. acs.est.8b03695 https://doi.org/10.1021/acs.est.8b03695 (2018).

70. Alam, M. S., Delgado-Saborit, J. M., Stark, C. & Harrison, R. M. Investigating PAH relative reactivity using congener profiles, quinone measurements and back trajectories. *Atmos. Chem. Phys.* **14**, 2467–2477 (2014).

Author contributions

S.S.G. conceived the research idea. M.Sh. and S.S.G. conceptualized the research experiments about plastic burning. R.S., S.S.G., S.N. and M.Sh. designed research. R.S., S.K., K.E., L.G., L.R.A., E.V., and R.R.K. performed experiments. R.S. and S.K. analysed the data. R.S., S.K., S.S.G., and M.Sh. interpreted the data. M.Sc. and M.Sh. conducted kinetic modelling. R.S., S.S.G. and M.Sh. wrote the paper with inputs from all coauthors.

Competing interests

The authors declare no competing interests.

Additional information

Supplementary information The online version contains supplementary material available at https://doi.org/10.1038/s44407-025-00015-8.

Correspondence and requests for materials should be addressed to Sachin S. Gunthe or Manabu Shiraiwa.

Reprints and permissions information is available at http://www.nature.com/reprints

Publisher's note Springer Nature remains neutral with regard to jurisdictional claims in published maps and institutional affiliations.